Theor Chem Acc (2003) 110: 130–143
DOI 10.1007/s00214-003-0474-y

Theoretical
Chemistry Accounts

Regular article

Modeling water exchange on monomeric and dimeric Mn centers

Marcus Lundberg, Margareta R. A. Blomberg, Per E. M. Siegbahn

Department of Physics, Stockholm Center for Physics, Astronomy and Biotechnology, Stockholm University, 106 91 Stockholm, Sweden

Received: 7 May 2002 / Accepted: 11 October 2002 / Published online: 10 October 2003

Abstract. Water exchange on Mn centers in proteins has been modeled with density functional theory using the B3LYP functional. The reaction barrier for dissociative water exchange on $[Mn^{IV}(H_2O)_2(OH)_4]$ is only 9.6 kcal mol^{-1}, corresponding to a rate of 6×10^5 s^{-1}. It has also been investigated how modifications of the model complex change the exchange rate. Three cases of water exchange on Mn dimers have been modeled. The reaction barrier for dissociative exchange of a terminal water ligand on $[(H_2O)_2(OH)_2Mn^{IV}(\mu\text{-}O)_2Mn^{IV}(H_2O)_2(OH)_2]$ is 8.6 kcal mol^{-1}, while the bridging oxo group exchange with a ring-opening mechanism has a barrier of 19.2 kcal mol^{-1}. These results are intended for interpretations of measurements of water exchange for the oxygen evolving complex of photosystem II. Finally, a tautomerization mechanism for exchange of a terminal oxyl radical has been modeled for the synthetic O_2 catalyst $[(terpy)(H_2O)Mn^{IV}(\mu\text{-}O)_2Mn^{IV}(O\bullet)(terpy)]^{3+}$ (terpy = 2,2′:6,2″-terpyridine). The calculated reaction barrier is 14.7 kcal mol^{-1}.

Keywords: Water exchange – Manganese – Dimers – Density functional theory

1 Introduction

To understand the reactivity of metal ions in biology and in solutions it is important to understand their exchange reactions and the most essential exchange reaction is exchange of water ligands. Results on this exchange process in the aqueous phase are widely available and have been reviewed recently [1]. In contrast, relatively little is known regarding water exchange in media other than water. This is unfortunate since knowledge about exchange reactions in enzymes can aid the interpretation of complex enzymatic mechanisms.

An intriguing example of water exchange in enzymes is given for the Mn_4 oxygen-evolving complex (OEC) in photosystem II (PSII) where exchange rates in the different S states have been investigated using ^{18}O-labeled water [2]. The two water molecules whose oxygens combine to form O_2 exchange with different rates in all S states. The highest exchange rate is greater than 175 s^{-1} and the lowest rate is 0.02 s^{-1} (at 10 °C), corresponding to barriers of less than 13.6 and 18.7 kcal mol^{-1}, respectively. The ultimate goal of that experimental study of exchange rates is to be able to attribute each exchange rate to a ligand position in the Mn_4 cluster.

The purpose of the present paper is to model water exchange on metal ions in enzymes rather than in water. This is to aid the interpretation of experiments like the one just described. One difference for metal centers in enzymes compared to the aqueous phase concerns the charge of the complex. In water solution, the charge on the metal complex is stabilized by the high dielectric constant. In biological systems, the metal center is often buried deep inside a low dielectric protein [3, 4, 5] where it is unlikely to carry a high charge. Consequently, neutral systems are chosen for the models in the present study. Since many enzymes have more than one metal ion [4, 5], the present article treats dimeric metal centers in addition to monomeric centers. This is a novel feature for a theoretical study at this level. Even larger complexes of metal ions exist, for example, the Mn_4 complex in PS II [6]. However, most aspects of the more complex systems are already present in the dimers. Regarding the choice of ligands, simple water derived (aqua, hydroxo and oxo) ligands have been used in the present models. These ligands have previously been used in theoretical studies of the OEC with good results [7]. Use of water-derived ligands makes it possible to calculate exchange rates not only for water ligands but also for hydroxo and oxo ligands, which should be present at different stages of the oxygen evolving reaction in the OEC.

Even though there are significant differences between exchange in proteins and aqueous solution, important

Contribution to the Björn Roos Honorary Issue

Correspondence to: M. Lundberg
e-mail: marc@physto.se

results can be obtained from previous studies. The standard classification of ligand-exchange reactions on monomers divides these into three different classes: dissociative (D) mechanisms, where an intermediate exists with a reduced coordination number, associative (A) mechanisms, where an intermediate exists with an increased coordination number, and intermediate (I) mechanisms, concerted reactions with no observable intermediate [8]. The latter can be divided into I_a and I_d, which are concerted reactions with associative and dissociative character, respectively. In the present paper, the I mechanism requires that the reaction proceeds through a single (and symmetrical) transition state [9]. The three mechanisms are shown schematically in Fig. 1.

Experimentally, exchange rates on first-row transition-metal ions in the aqueous phase span 15 orders of magnitude [1]. Owing to the large range of rates, different experimental and theoretical methods have been used to shed light on water exchange processes. Among the theoretical methods, Hartree–Fock and complete-active-space self-consistent field have been applied to all first-row transition metals with good results [10]. Since the present paper focuses on Mn, previous results for this metal are of particular interest here. $[Mn^{II}(H_2O)_6]^{2+}$ was found to exchange with an A mechanism and the calculated barrier $\Delta E^{\ddagger}$, was 7.4 kcal mol^{-1} [10]. This is in good agreement with the experimental barrier, $\Delta G^{\ddagger}$, of 7.5 kcal mol^{-1} (rate of $2.1 \times 10^7\, s^{-1}$) [11]. In the same theoretical study it was found that exchange on $[Mn^{III}(H_2O)_6]^{3+}$ proceeds via a D mechanism with a barrier of 12.9 kcal mol^{-1}. An associative exchange mode for Mn^{III} has also been studied theoretically [12], but the barrier was slightly higher. In general, the character of the exchange mechanism changes from associative to dissociative as the ionic radius decreases and the number of 3*d* electrons increases [1, 10].

The present study uses density functional theory (DFT). DFT calculations have previously been applied to several water-exchange reactions [13, 14, 15, 16]. An interesting observation from one of the studies is that with a hydroxo ligand instead of an aqua ligand in the first shell of Ti^{2+} the exchange mechanism (for a water ligand) changed from A to D [15]. At the same time, the reaction barrier decreased by 6 kcal mol^{-1}. The decreased barrier for exchange of an aqua ligand can either be attributed to a trans effect from the strongly bound hydroxo or to a decrease in the charge of the metal complex (from +2 to +1). Extrapolating this result to the Mn^{III} results mentioned earlier, an expected barrier of $12.9 - 6.0 = 6.9$ kcal mol^{-1} is obtained for a Mn^{III} monomer with a hydroxo ligand. This result is relevant for the present study since hydroxo ligands are used to achieve charge neutrality.

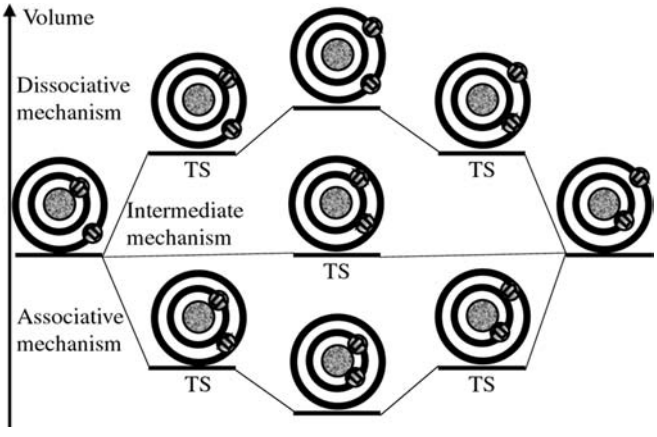

Fig. 1. Schematic picture of the associative (*A*), dissociative (*D*) and intermediate (*I*) mechanisms for ligand exchange between first and second coordination shells

In all the studies mentioned earlier, the first coordination shell was treated at a high level of theory. Including also a complete second shell is more problematic. In Cr^{III}, which has been carefully investigated, the second shell consists of at least 12 water molecules [17]. Including a full second shell in the quantum mechanical calculations seems to have been attempted [14] but no results have been presented. The most common approach is to include a single second shell water in the high-level models and to treat the rest of the surroundings in an approximative way. Deeth and Elding [13] used simple Born approximations and molecular modeling simulations to estimate the effect of the surroundings and found that they were quantitatively similar. Another alternative is to use polarizable continuum model (PCM) methods that account for multipoles [18]. The present study uses a single second shell water and treats the surroundings as a homogeneous medium using the conductor-like PCM (CPCM) method [19, 20].

As already mentioned, a theoretical study found a labilizing effect when a hydroxo ligand was introduced into the first shell. This effect had earlier been observed experimentally for both monomers and dimers [21, 22, 23, 24]. Water-exchange barriers on Cr^{3+} decreased by 4 kcal mol^{-1} by including a hydroxo ligand in the first shell [21]. A bridging hydroxo ligand on the Cr^{3+} dimer had a slightly smaller effect (2 kcal mol^{-1}) [22]. A similar trend was found for Rh^{III}. A hydroxo ligand in the first shell of the monomer decreased the exchange barrier by 3–4 kcal mol^{-1} [23, 24]. Ligands trans to the hydroxo bridge in the dimer $[Rh^{III}(\mu\text{-}OH)_2Rh^{III}]^{4+}$ exchanged dissociatively with a barrier 1–2 kcal mol^{-1} lower than the barrier in the hexaaqua-coordinated monomer. No exchange of the bridging OH groups could be detected [24]. The single μ-oxo bridge of the Ru-dimer *cis*,*cis*-$[(bpy)_2Ru(H_2O)]_2^{4+}$ does not seem to exchange either [25, 26]. In cases where exchange of bridging ligands has been detected, rates are in general low. Exchange of the bridge in $[Cr^{III}(\mu\text{-}OH)_2Cr^{III}]$ has a barrier of 24.3 kcal mol^{-1} (rate of 10^{-5} s^{-1}) [22]. Finally, exchange of the μ-oxo bridge in the iron dimer of the enzyme ribonucleotide reductase has a barrier of 21.7 kcal mol^{-1} [27]. This is within a few kilocalories per mole of the barrier of the slowly exchanging water in the S_3 state of the OEC and calculated exchange barriers for μ-oxo bridges are expected to be in this range.

2 Computational details

The calculations in the present study were performed in three steps. Following an optimization of the geometry with a rather small

basis set, the energy is calculated using a larger basis set. In the third step, thermal effects and the effect from the polarized surrounding are added to the energy. All the calculations used the DFT hybrid functional B3LYP [28, 29]. Gaussian98 [30] was used for most of the calculations, but large basis set calculations on Mn dimers were performed using Jaguar [31].

In the geometry optimizations, the LANL2DZ basis set was employed. This basis set is a d95 basis set (double-zeta quality) [32] with a nonrelativistic effective core potential (ECP) [33] for Mn atom. This rather small basis set can be used with good results since it has been shown that the final energy is rather insensitive to the quality of the geometry optimization [34]. Optimized structures are accepted if the Hessian (i.e. second derivatives of the energy with respect to the nuclear coordinates) only has positive eigenvalues. The Hessians are also used to estimate zero-point, thermal and entropy effects on the relative energies, applying the harmonic approximation. Transition states (TS) are obtained by full optimizations following a Hessian calculation. TS are characterized by Hessians with a single negative eigenvalue corresponding to the reaction coordinate.

Following the geometry optimization, the energy is calculated using the all-electron basis set 6-311 + G(d,p), with polarization functions added to all atoms and diffuse functions added to the heavy atoms. For the antiferromagnetically coupled dimers, it is sometimes difficult to get convergence for the all-electron basis set. To get consistent results, the LACV3P**+ basis set from the program Jaguar was used for all the energy calculations on the Mn dimers. The LACV3P basis set is of triple-zeta quality and uses an ECP [33] for the Mn atom.

Regarding the rather small basis set in the geometry optimization, Hartmann et al. found a TS for water exchange if they optimized without hydrogen p functions that could not be localized with the p function added [14]. This is also the case in the present study (for reaction 8) but it is not very important since the energy obtained from the large basis set calculation shows if the calculated TS is not a true TS on the potential-energy surface.

The part of the surroundings that is not explicitly included in the model is treated as a homogeneous medium with a dielectric constant of 4. The value of the dielectric constant is chosen in line with previous suggestions for proteins. The choice is arbitrary but has previously been shown to give results in good agreement with experimental data [35]. In general, the dielectric effects are rather small and the effect of changing the ϵ value is therefore expected to be small. The CPCM polarizable conductor model (Cosmo) [19, 20] is used and the radii of the solvent molecules are taken from the parameters for water.

The inherent accuracy of the B3LYP method has been estimated using the extended G3 benchmark set [36]. This test has 376 entries, and the B3LYP functional obtains an average error of 4.27 kcal mol^{-1} [36]. However, the main part of the entries in the benchmark test is concerned with enthalpies of formation for molecules of various sizes. Errors in enthalpies of formation, where many new bonds are formed, are not very relevant when studying reaction mechanisms where no covalent bonds are formed. The energetics of the water-exchange processes should be less prone to errors than enthalpies of formation. In addition, the relative errors when comparing the same type of exchange reactions should be even less prone to errors. An estimated error from the B3LYP treatment is 1–2 kcal mol^{-1} for the relative barriers.

Benchmark calculations using the same methods and basis sets as in the present paper gave a barrier 2.5 kcal mol^{-1} too high when applied to water exchange on $Fe^{3+}(H_2O)_6$ (10.9 versus 8.4 kcal mol^{-1} experimentally [1]). By extending the number of water molecules in the second coordination shell to 2 and 3, the calculated barrier dropped, but only by 0.5 kcal mol^{-1}. No results were obtained for more than three water molecules in the second shell.

Finally, DFT calculations on low-spin coupled open-shell systems, for example, antiferromagnetic coupling of two high-spin Mn^{IV} centers, do not give the correct energy. To be able to correct the energy of the low-spin state, both high-spin and low-spin states should be calculated. A $\boldsymbol{J}$ value can then be obtained using the Heisenberg Hamiltonian formalism [37]. In principle, the correction should be applied to all dimers with antiferromagnetic coupling. In the present study it is assumed that the correction is approximately constant throughout the water-exchange reactions. It is therefore not included for dimers that keep their antiferromagnetic coupling throughout the reaction. However, in the last part of the Results section, exchange of a terminal oxo group is proposed to proceed via a ferromagnetic state. For this system, the correction to the antiferromagnetic state is calculated since the energy difference between antiferromagnetic and ferromagnetic states enters directly in the barrier.

3 Results

Biological systems with transition metals are diverse with a large selection of different ligands and oxidation states. It is not feasible to model all these variations. Instead, the approach in the present paper is to start with a very simple neutral Mn^{IV} complex with water-derived ligands. Modifications and additions are made for this model to estimate relative effects on the exchange rate. In the first part, effects of changes in ligand composition and oxidation state of the monomer are studied. In the second part, attention is turned from monomers to dimers and exchange reactions on the bimetallic centers Mn^{IV}–Mn^{IV} and Mn^{IV}–Ca^{II} are modeled. For the former, exchange rates of a terminal water ligand and a bridging oxo group are studied. Finally, the tautomerization exchange mechanism for a terminal oxo group in a Mn dimer is investigated.

3.1 Ligand exchange on monomeric Mn centers

3.1.1 Water exchange on $[Mn^{IV}(H_2O)_2(OH)_4]H_2O$ (reaction 1)

Exchange on a Mn^{IV} center has not been studied previously since this oxidation state is unstable in water. In biology, it is proposed to be an important oxidation state in the reaction sequence of OEC [6]. Throughout the present study, Mn^{IV} is modeled as a high-spin ^4A state in line with previous modeling experience [38]. The model complex is chosen to be neutral. To compensate for the charge on the Mn ion, four negative ions (hydroxides) are therefore included in the first coordination shell. A single water molecule is located in the second coordination shell.

There are several possible configurations for the reactant. The strategy for locating the global minimum mainly takes three effects into account. The first priority is to consider trans effects and position tightly binding ligands (hydroxides) trans to loosely bound ligands (water) to the greatest possible extent. The second priority is to optimize the hydrogen bond strengths. The second-shell water makes two hydrogen bonds. It should donate a bond to the best proton acceptor (a loosely bound hydroxo ligand), which in the Mn^{IV} system is a hydroxo ligand trans to ano\ther hydroxo. The water molecule should also receive a bond from the best proton donor (the tightest bound water). Rotations of the ligands also create local minima that have to be avoided. The final structure of reactant 1 is shown in Fig. 2.

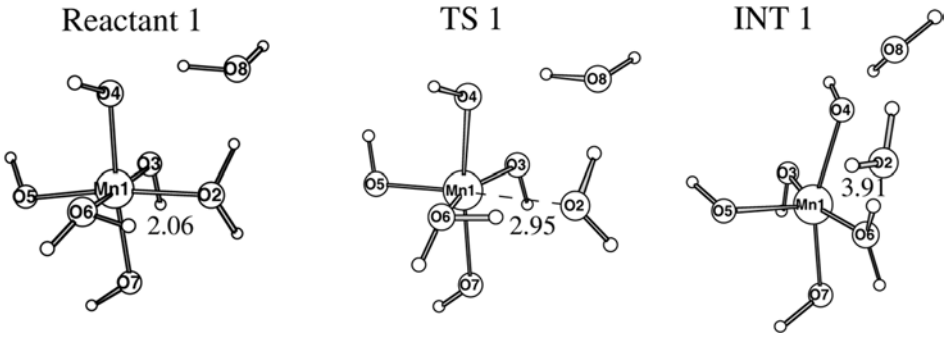

Fig. 2. Structures of reactant, transition state (*TS*) and intermediate encountered during water exchange on $[Mn^{IV}(H_2O)_2(OH)_4]H_2O$ (reaction 1). The *numbers* represent the relevant Mn–O distance in angstroms

Mn^{IV} has three electrons in its 3*d* orbitals and according to the findings on hexaaqua-coordinated centers [10], Mn^{IV} should substitute by the A or I_a mechanism. In contrast, the present study found that the D mechanism has the lowest barrier for water exchange on $[Mn^{IV}(H_2O)_2(OH)_4]H_2O$ (reaction 1). The first TS (TS 1 in Fig. 2) has a distance between Mn1 and the exchanging water ligand O2 of 2.95 Å.

TS 1 represents the leaving water molecule (O2) going from the first to the second coordination shell. The barrier is 9.6 kcal mol^{-1}. An intermediate (INT 1) is formed with two water molecules in the second shell (Fig. 2). This intermediate is rather stable and lies only 3.3 kcal mol^{-1} above the reactant. A second TS on the energy profile (TS 1*) represents the incoming water (O8) going from the second to the first coordination shell. As the product is identical to the reactant, the reaction is symmetric. The second TS (TS 1*) is therefore identical but reverse to the first TS (TS 1) and has the same barrier. Throughout the present paper, structures labeled with asterisks (e.g. TS 1*) correspond to an earlier structure on the reaction path (e.g. TS 1), however, with leaving and incoming ligands interchanged. For the same symmetry reason, the overall reaction is thermoneutral. The energy profile of the reaction is shown in Fig. 3. The five species in the energy profile correspond to the five structures shown for the D mechanism in Fig. 1.

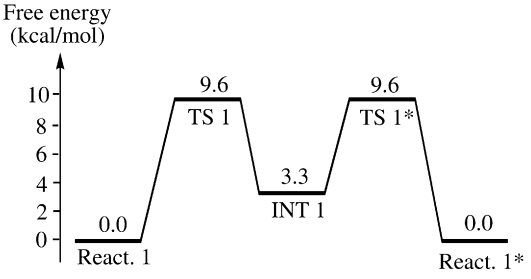

Fig. 3. Energy profile including the TS and the intermediate for the D water exchange reaction on Mn^{IV} (reaction 1). The general shape of the energy profile is the same for all D mechanisms in the present study

No other low-energy TS could be found on the potential-energy surface for water exchange. To confirm the validity of the dissociative mechanism, a 2D energy surface was constructed by scanning the two Mn–OH_2 distances (Fig. 4). The surface represents all mechanisms for exchange of the two water molecules in different shells (in this model), except an associative mechanism with attack trans to the leaving water. It clearly shows a dissociative reaction with two transition states. The energy profile in Fig. 3 was obtained by following the edges of the surface in Fig. 4. Preference for the D mechanism in neutral systems is not entirely surprising. As mentioned in the Introduction, a similar effect has been observed with one hydroxide in the first coordination shell [14, 23, 39].

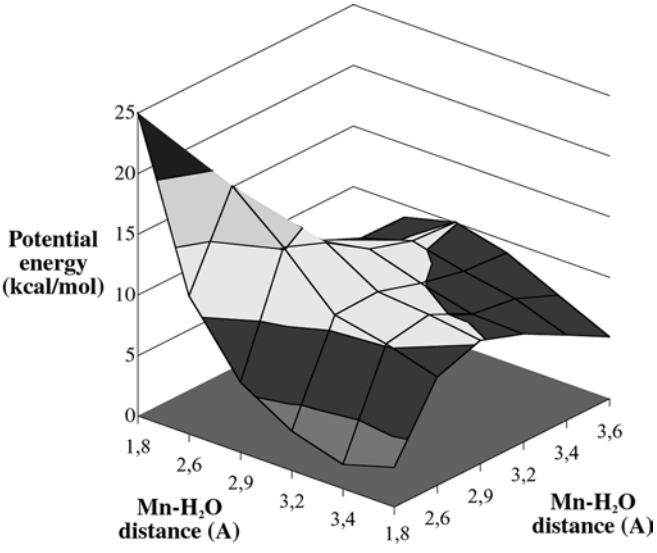

Fig. 4. The two-dimensional energy surface for the water-exchange reaction on $[Mn^{IV}(H_2O)_2(OH)_4]H_2O$ (reaction 1) obtained by scanning the two Mn–OH_2 distances. Compare the shape of the surface with the energy profile in Fig. 2. Note that for short bond distances (1.8–2.6 Å) the axes are compressed and the energy scale does not show values above 25 kcal mol^{-1}

3.1.2 Water and hydroxide exchange on $[Mn^{IV}(H_2O)_2(OH)_3(Cl)]H_2O$ (reactions 2 and 3)

When hydroxo ligands are included in the first shell, at first it seems reasonable that exchange rates for these hydroxo ligands can be obtained. The problem is that in models with only water-based ligands different exchange rates for hydroxo ligands compared to water ligands is not a meaningful concept. Rearrangement of protons between water and hydroxo ligands is predicted to occur much faster than exchange, thus making the ligands

Table 1. Energies (kcal mol^{-1}) for structures along the reaction path for water exchange between the first and the second coordination shell. The values of ΔE do not include corrections from solvent, zero-point and thermal effects

Metal center	Reaction	TS		INT	
		$\Delta E^{\ddagger}$	$\Delta G^{\ddagger}$	ΔE	ΔG
$[Mn^{IV}(H_2O)_2,(OH)_4]H_2O$	1	7.6	9.6	1.4	3.3
$[Mn^{IV}(H_2O)_2(OH)_3(Cl)]H_2O$	2	8.8	10.8	2.2	4.3
$[Mn^{III}(H_2O)_2(OH)_3]H_2O$	4	5.9	6.3	−1.8	−1.6
$[Mn^{III}(H_2O)_2(OH)_2(Cl)]H_2O$	5	7.2	9.5	0.7	3.9
$[(H_2O)_2(OH)_2Mn^{IV}(\mu\text{-}O)_2$ $Mn^{IV}(H_2O)_2(OH)_2]H_2O$	6	8.4	8.6	8.0	5.8

equivalent. However, adding a non-water ligand creates a distinctly different position trans to this ligand. A simple way to model this is to replace one of the OH^- ions with a Cl^- ion. To check the effect of a Cl^- ion on water exchange, the barrier for water exchange was calculated again, now with Cl^- cis to the exchanging water (reaction 2). The new barrier is 10.8 kcal mol^{-1}. The change in reaction barrier compared to reaction 1 is not negligible ($\Delta\Delta G^{\ddagger} = 10.8 - 9.6 = 1.2$ kcal mol^{-1}). Results for water exchange on all types of centers are summarized in Table 1.

Going back to hydroxide exchange on Mn^{IV}, a picture of the model with atomic labels is shown in Fig. 5. The most interesting ligand is the one trans to the Cl^-, that is O4. The complex is 3.0 kcal mol^{-1} stables with a hydroxo ligand in this position compared to an aqua ligand. It is this hydroxo ligand that will be exchanged. Since a hydroxide ion is less stable than a water molecule in the second shell, the exchanging hydroxide must receive a proton during the exchange reaction. In this model, the proton donor is a water ligand (O2) and the transfer is mediated by the water in the second shell (O8). The proton transfer is modeled as a separate step and has a barrier of 5.2 kcal mol^{-1}. The TS (TS 3a) is the structure shown in Fig. 5. After passing the TS, O4 now becomes a water molecule. This intermediate (INT 3a) lies 3.0 kcal mol^{-1} above the reactant, owing to less optimal trans effects in INT 3a compared to reactant 3. In the second step, the "new" water molecule O4 exchanges in a D mechanism, exactly as for reaction 1. O4 leaves for the second shell and O8 comes in to bind to the Mn ion. The total barrier for hydroxide (O4) exchange

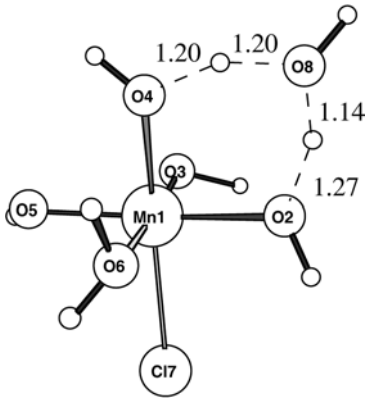

Fig. 5. TS 3a represents proton transfer from a water ligand (O2) to a hydroxo ligand (O4) via a water molecule in the second shell (O8). The *numbers* represent distances in angstroms

is 13.6 kcal mol^{-1}. This is 13.6−10.8 = 2.8 kcal mol^{-1} higher compared to water exchange on the same center (reaction 2). All of this energy difference comes from the energy to protonate the hydroxide. Exchange rates of hydroxides thus depend directly on the availability of proton donors.

3.1.3 Water exchange on $[Mn^{III}(H_2O)_2(OH)_3]H_2O$ (reaction 4)

Changing the oxidation state of the Mn center has several implications. Apart from the lower charge, Mn^{III} is expected to behave differently compared to Mn^{IV} since it is Jahn–Teller (JT) active. The ligands that coordinate along the JT axis are weakly bonded compared to the four ligands in the perpendicular plane. Indeed, when optimizing the six-coordinated structure, one ligand along the JT axis is actually lost to the second coordination shell, resulting in a preference for a five-coordinated species. The final model thus includes five ligands in the first shell and one water molecule in the second shell. The model is designed according to the rules mentioned earlier for Mn^{IV}. The remaining ligand along the JT axis must be a water molecule. Exactly as for Mn^{IV}, the mechanism is dissociative. For Mn^{III} the reaction barrier is 6.3 kcal mol^{-1}. This is 3.3 kcal mol^{-1} lower than the same reaction (reaction 1) on Mn^{IV} ($\Delta\Delta G^{\ddagger} = 6.3-9.6 = -3.3$ kcal mol^{-1}). In the TS, the Mn–OH_2 distance is 2.63 Å. A four-coordinated intermediate exists 1.6 kcal mol^{-1} below the reactant. The stability of this low coordination number is unexpected. One explanation is that calculations with a relatively small basis sets overestimate the hydrogen bond strengths and are therefore biased towards structures that form more hydrogen bonds. If this is the case, it influences all the calculations in the present study (see Discussion). Another possibility is that there exists a stabler five-coordinated structure that despite several attempts has not been found. If this is the case, the barrier for exchange on Mn^{III} would be higher.

Starting with a five-coordinated species, the A mechanism should be interesting since its intermediate is six-coordinated. Indeed, the A mechanism is possible with a stable six-coordinated intermediate 3.9 kcal mol^{-1} above the reactant. It is not straightforward to find the TS, but it seems that it lies approximately 8 kcal mol^{-1} above the reactant. Since this is higher than the barrier for the D mechanism, the A mechanism is not considered to be very important. No TS corresponding to the I_a mechanism could be found, neither for an attack cis to the leaving water nor trans to it.

3.1.4 Water exchange on $[Mn^{III}(H_2O)_2(OH)_2(Cl)]H_2O$ (reaction 5)

By adding a Cl^- ion instead of one of the OH^- ions on Mn^{III} the barrier increases by 3.2 kcal mol^{-1} from 6.3 to 9.5 kcal mol^{-1}. This is larger than the corresponding effect on the Mn^{IV} center, where a Cl^- ion increased the barrier by 1.2 kcal mol^{-1} (reaction 2 compared to reaction 1).

3.2 Ligand exchange on dimeric centers

Many metal centers in proteins exist as dimers or more advanced configurations of metal ions [4, 5, 6]. Modeling dimers is sufficient at this stage since many positions in the more complex configurations appear already in the dimer. Several different bridging modes are possible for metal dimers but for Mn dimers only the rather common bis-μ-oxo bridge will be considered here. A dimer with this configuration has three distinctly different positions for the ligands: first are the bridging ligands (μ-oxo); second are the positions trans to the bridging oxo groups; and third are the positions cis to the bridging oxos. All these three positions exchange differently compared to the monomer, as shown experimentally for the dihydroxo-bridged Rh^{III} dimer [24].

In the present paper, a Mn dimer is modeled using two high-spin Mn^{IV} centers antiferromagnetically coupled yielding a ^{1}A state. All ligands are water derivatives; μ-oxo, hydroxo or water. The composition of the ligands in the complex is chosen to keep the complex neutral. The positions and orientations of the ligands are chosen as argued previously. Each bridging oxo group has two other ligands in trans positions but both of them are not weakly bonded ligands.

One water molecule is located in the second shell. A difference compared to the monomers is that in the dimer models, the position of the water in the second shell does not always correspond to the lowest energy. For the dimer models, the second-shell water is put in positions where it is able to participate directly in the exchange reactions. It is assumed that the other positions in the second shell are already occupied by other molecules. Reactants for exchange of a terminal water ligand

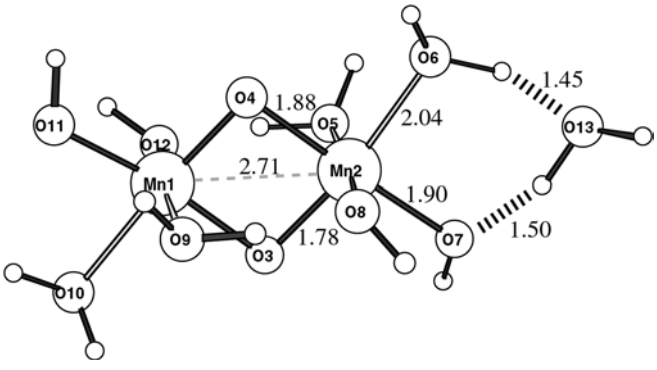

Fig. 6. Reactant used to model terminal water exchange on $[(H_2O)_2(OH)_2Mn^{IV}(\mu\text{-}O)_2Mn^{IV}(H_2O)_2(OH)_2]H_2O$ (reactant 6). The *numbers* represent distances in angstroms

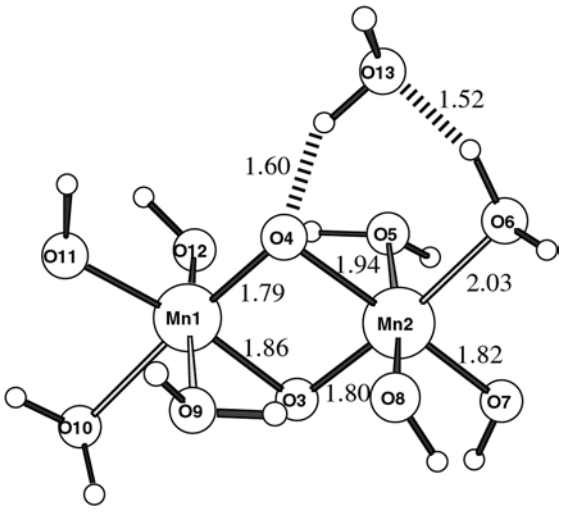

Fig. 7. Reactant used to model exchange of a μ-oxo bridge on a Mn dimer $[(H_2O)_2(OH)_2Mn^{IV}(\mu\text{-}O)_2Mn^{IV}(H_2O)_2(OH)_2]$ (reactant 7). The numbers represent distances in angstroms

(reactant 6) and a bridging oxo group (reactant 7) are shown in Figs. 6 and 7, respectively.

3.2.1 Terminal water exchange on $[(H_2O)_2(OH)_2Mn^{IV}(\mu\text{-}O)_2Mn^{IV}(H_2O)_2(OH)_2]H_2O$ (reaction 6)

The position trans to the oxo group is rather similar to the positions of the water ligands on the monomer. In one of these positions, water (O6) is a stable ligand. For labels in this section see Fig. 6. A water in the second shell (O13) is located in a position where it can easily exchange with the terminal water. Apart from the position of the exchanging water, it was important to get the hydrogen-bonding pattern correct. The proton on the water ligand O5 must point towards the leaving water (O6) since it will form an important hydrogen bond in the TS and in the intermediate, and it cannot rotate easily owing to the hydrogen bond to O12. The orientation of the other proton on O5 is not optimal compared to reactant 7, but the energy difference is rather small (0.7 kcal mol^{-1}). This modeling issue does not appear for reactions on monomers since their water molecules are not fixed by any hydrogen bonds.

Instead of trying all different mechanisms (D, I and A) of the terminal water O6, it was assumed that exchange on this position resembles that on the Mn^{IV} monomer. There is no reason to suspect that the A mechanism should be favored when going from monomer to dimer. As expected, the calculations locate a TS (TS 6 shown in Fig. 8) corresponding to the D mechanism. The barrier is 8.6 kcal mol^{-1}. Compared to the monomer (reaction 1), the Mn–O bond distance is slightly longer at the TS (2.98 compared to 2.95 Å) and the reaction barrier is 1.0 kcal mol^{-1} lower ($\Delta\Delta G^{\ddagger} = 8.6 - 9.6 = -1.0$ kcal mol^{-1}). By following the reaction coordinate, a stable intermediate (INT 6) is found 5.8 kcal mol^{-1} above the reactant. INT 6 is less stable than the corresponding intermediate on the monomer (INT 1), especially when looking only at the electronic energy (Table 1). This can be explained by

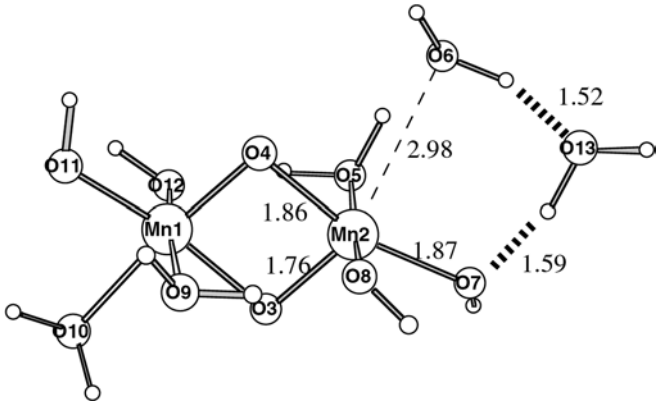

Fig. 8. TS for exchange of terminal water ligand position on a bis-μ-oxo dimer (TS 6). The *numbers* represent distances in angstroms

the loss of rotational flexibility of the water ligands in INT 6 which leads to less optimal hydrogen bonds compared to INT 1. All the results for exchange of water ligands are shown in Table 1.

A and I_a mechanisms were not as thoroughly investigated, i.e. no fully optimized transition states were calculated. Since seven-coordination was not stable for any monomeric Mn center, the A mechanism was ruled out. An I_a mechanism was attempted where the terminal water ligand O6 is attacked by an incoming water cis to the leaving ligand. This mechanism has a barrier of approximately 14 kcal mol^{-1}. This should be compared to 8.6 kcal mol^{-1} for the D mechanism and the I_a mechanism was therefore ruled out.

3.2.2 Exchange of a bridging oxo group on $[(H_2O)_2(OH)_2Mn^{IV}(\mu\text{-}O)_2Mn^{IV}(H_2O)_2(OH)_2]H_2O$ (reaction 7)

The exchange of the bridging oxygen has no direct analogue in the monomer. The interpretation of the possible reaction mechanisms must therefore be different, although some similarities exist.

To participate in an exchange reaction the oxo group (O4 in Fig. 7) must receive two protons and the first question is at which stage these protonations occur. It is proposed here that the first step of the reaction is a single protonation of the oxo bridge. The protonation could proceed from the terminal water O6 via the water in the second shell (O13) in analogy to TS 3a in Fig. 5. However, in the calculations the proton is taken from a water ligand (O10) on the other Mn ion. In this way, the second protonation of the bridging ligand can occur from the terminal water O6. The transfer of a proton from the terminal O10 to the bridging O4 is exothermic by 2.9 kcal mol^{-1}, i.e. a protonated bridge is the stablest configuration. This is different from the experimental results obtained for the highly oxidized Mn dimers in PSII which are known to have unprotonated bridges. The preference for a protonated bridge in the present model is probably not an error in the DFT calculations but is due to the choice of ligands. A comparison is made with the Mn dimer $[(terpy)(H_2O)Mn(O)_2Mn(OH_2)(terpy)]^{n+}$ (terpy = 2,2′:6,2″-terpyridine) which has a tridentate terpyridine ligand and a water ligand at each center. The complex is further investigated in a later section of the present paper. For this terpy-Mn dimer protonation of the bridge was endothermic (by 3.9 kcal mol^{-1} in the Mn^{IV}–Mn^{III} oxidation state), which is in line with experimental data.

The energy of the first protonation step is important. If the step is endothermic, the protonation energy enters directly into the barrier for water exchange. Since the origin of the proton is not known and the energy of the step depends on the unknown ligands, it is assumed to be thermoneutral. In this way, the energy required to protonate the bridge can simply be added to the barrier.

Going back to the model structure which now has a bridging hydroxo ligand (INT 7a in Fig. 9), there are several possibilities for the exchange of this hydroxo group. All these mechanisms start from reactant 7, shown in Fig. 7.

Guided by the experience from the studies on the monomer, a D mechanism was initially investigated: this is the ring-opening mechanism shown in Fig. 9. In the first step, the bridging ligand (O4) leaves one of the centers (Mn2) and coordinates only to the other. To

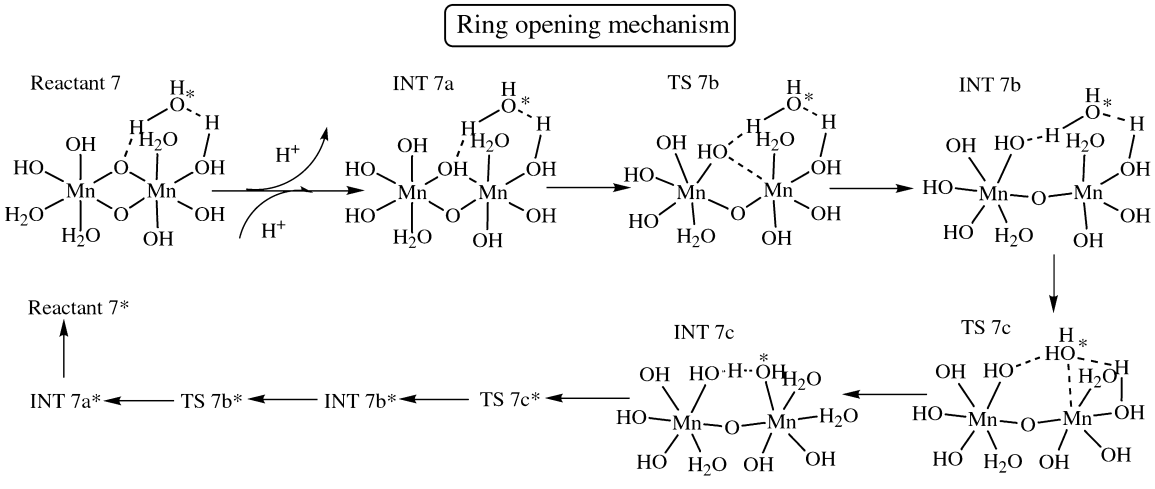

Fig. 9. The suggested mechanism for exchange of a bridging oxo group in a Mn dimer

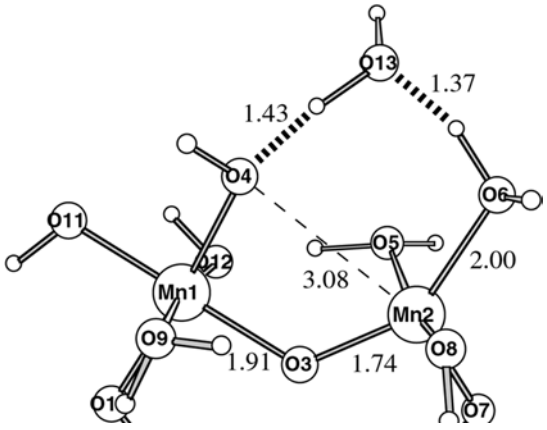

Fig. 10. TS (TS 7b) for exchange of a bridging oxo group. The *numbers* represent distances in angstroms. The reaction coordinate is the bond between Mn2 and the leaving hydroxide O4

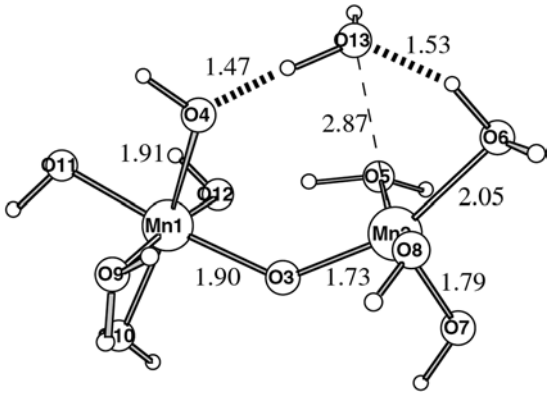

Fig. 11. TS (TS 7c) for exchange of a bridging oxo group. The *numbers* represent distances in angstroms. The reaction coordinate is the bond between Mn2 and incoming water O13

reach that structure, the TS shown in Fig. 10 (TS 7b) must first be passed. The reaction barrier is 19.2 kcal mol^{-1} and the distance between Mn2 and the leaving ligand O4 is 3.08 Å. By following the reaction coordinate from TS 7b, INT 7b is reached at an energy of 11.9 kcal mol^{-1}. INT 7b has a six-coordinated Mn (Mn1) and a five-coordinated Mn (Mn2). The Mn ions are bridged by a single oxo group (O3). This first step is identical to the mechanism proposed for exchange of the bridge in $[Cr^{III}(\mu\text{-}OH)_2Cr^{III}]$ [22].

In INT 7b, the five-coordinated Mn2 is ''open'' for attack by the external water ligand (O13). This attack corresponds to the incoming ligand in the D mechanism on the monomer and in the dimer model it proceeds over a barrier of 19.1 kcal mol^{-1} (TS 7c shown in Fig. 11). Passing the TS results in a third intermediate (INT 7c) where both Mn are six-coordinated but there is still only one bridging oxo group (O3). In this structure, a proton is almost equally divided between the incoming water (O13) and the formerly bridging ligand (O4). INT 7c lies 4.9 kcal mol^{-1} above reactant 7.

From INT 7c, the reaction is proposed to proceed in a symmetric fashion. O4 takes the proton shared with O13 in INT 7c and leaves the direct coordination to Mn1. O4 ends up in the second shell followed by a closing of the ring by turning O13 into a bridging ligand. The overall result is that the water in the second coordination shell (O13) has become a bridging ligand, while the former bridging ligand (O4) now resides in the second shell. The energy profile of the entire reaction is given in Fig. 12.

Several other mechanisms for exchange have been investigated, although not as thoroughly as that just described. Studies were made on even more D mechanisms where two five-coordinated Mn-centers are created. From INT 7a one alternative is to supply the bridging hydroxo O4 with a second proton, this time from the terminal water O6. The cost of protonating the bridging oxo group a second time is 14 kcal mol^{-1} (LANL2DZ basis set). The bridging water can now move directly to the second shell. This step has an estimated barrier of 12 kcal mol^{-1}, rendering a total barrier of $14+12=26$ kcal mol^{-1} higher than the ring-opening mechanism. Another possibility follows the suggestion for the Cr dimer [22]. The first steps leading to INT 7b are the same as for the previously described ring-opening mechanism. At INT 7b the hydroxo ligand O4 receives its second proton. This is followed by rotation of Mn1 around the single oxo bridge before the ring closes. O4 has now become a terminal ligand. In the present model, rotation of Mn1 is hindered by two strong hydrogen bonds between the ligands on Mn1 and Mn2. This barrier, which has not been estimated, should be added to the energy of INT 7b that already lies more than 11.9 kcal mol^{-1} above the reactant. Even if the rotation can be accomplished, terminal exchange of O4 would have a barrier approximately 8.6 kcal mol^{-1} above INT 7b. Compared to the reactant, the total barrier for this mechanism is thus around 21 kcal mol^{-1} ($8.6+11.9$ kcal mol^{-1}). This indicates that the rotation mechanism is not significantly better than the ring-opening mechanism previously described.

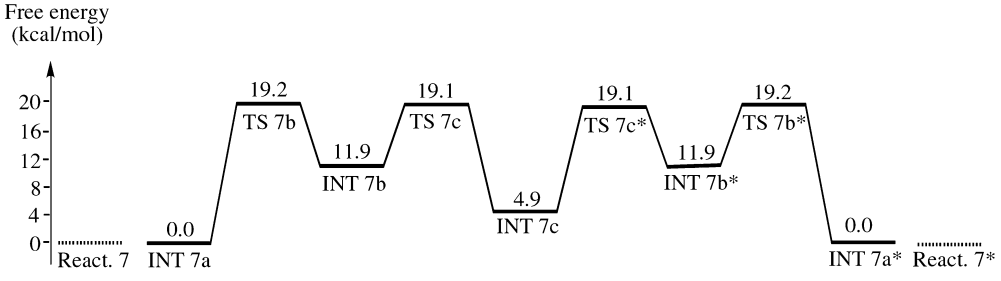

Fig. 12. Potential-energy profile for the ring-opening mechanism for exchange of a bridging oxo group on a Mn^{IV}–Mn^{IV} dimer (reaction 7)

Two different I_a mechanisms have been attempted. Both start from the structure with the bridging hydroxo (INT 7a). The first is similar to the I_a mechanism of the monomer with a water (O13) attacking directly at Mn2. Since the seven-coordinated A intermediate is not stable, the desired result is a concerted cleavage of the bond between Mn2 and the bridging hydroxo O4. That would lead to the direct creation of INT 7c with two six-coordinated Mn ions. It should be noted that an associative attack by a water in the second shell easily causes the terminal water O6 to be ejected before the bridging ligand leaves. This is expected because exchange of a terminal ligand is easier than exchange of a bridging ligand. To explore the I_a exchange of a bridging ligand, the potential-energy surface was scanned by varying the Mn2–O4 and Mn2–O13 bond distances. The relevant part of the potential-energy surface is the one where ejection of the terminal water O6 is avoided. The TS is the lowest stationary point on this surface and this point is estimated to lie 25 kcal mol^{-1} above the reactant.

The second I_a mechanism that was investigated is more symmetrical with regard to the two different metal centers. Here water in the second shell attacks the bridging hydroxo O4 in the plane perpendicular to the Mn–Mn bond. In the TS, the incoming (O13) and the leaving ligand (O4) are symmetrically bonded to the two Mn centers. Since the two ligands are indistinguishable at this point, one of the protons that initially resided on the incoming water O13 is divided equally between O4 and O13 in the TS. A rough investigation of the potential-energy surface gave an estimate of 30 kcal mol^{-1} for the barrier.

3.2.3 Exchange of a bridging hydroxo ligand on $[(H_2O)(OH)_3(Cl)Mn^{IV}(OH)Ca^{II}(H_2O)_4(OH)]$ (reactant 8)

In addition to the homometallic dimer, a dimer with two different metal centers was studied. A Mn^{IV}–Ca^{II} dimer was chosen, mainly because both metals are present together in the OEC of PSII.

Owing to the rather weak interaction between the metals, it is predicted that formation of a Mn–Ca dimer does not change the exchange rate significantly for those ligands that do not reside between the metal ions. Only exchange of a bridging ligand was investigated and the present Mn^{IV}–Ca^{II} dimer has only one bridging ligand. This position is occupied by a hydroxo group. Exchange of a hydroxo group was previously modeled for the Mn^{IV} monomer with Cl^- added to the complex (reaction 3). To get a similar system, Cl^- is added as a ligand to Mn^{IV} also in the Mn^{IV}–Ca^{II} dimer. The reactant is shown in Fig. 13. In this reactant, no water molecule is added to the second shell. Calculations show that it is more favorable if the incoming ligand is a ligand to Ca (O9 in Fig. 13) rather than a second-shell water. Ignoring the second shell also avoids artificial changes in hydrogen bonding during the final stages of the reaction.

By analogy with the exchange of a hydroxo ligand on the monomer (reaction 3), the first step is to protonate the bridging hydroxo group (O4 in Fig. 13). A reaction mechanism was modeled where the proton donor is the water ligand O6. In order to get a TS for this reaction, a water molecule must be present in the second shell and such a water molecule was therefore added for this specific step. The TS (TS 8a) is very similar to the TS for proton transfer on the monomer (Fig. 5). After passing the TS, O4 becomes a water molecule and leaves its coordination to Mn1. This second reaction step is modeled without a water molecule in the second coordination shell as already mentioned. The structure passes through TS 8b shown in Fig. 14 with a barrier of 10.4 kcal mol^{-1}. After this TS is passed, an intermediate (INT 8b) is formed where O4 coordinates to Ca. Now the Ca-coordinated O9 attacks the five-coordinated Mn and becomes the bridging ligand after losing its proton to O6. O4 that was initially bridging now resides in the first coordination shell of Ca, a position from where it can easily exchange.

Comparing the two results for exchange of a hydroxo ligand (reactions 3 and 8) shows that Ca actually decreases the barrier by 13.6 – 10.4 = 3.2 kcal mol^{-1}. A summary of the results for hydroxo ligands is given in Table 2.

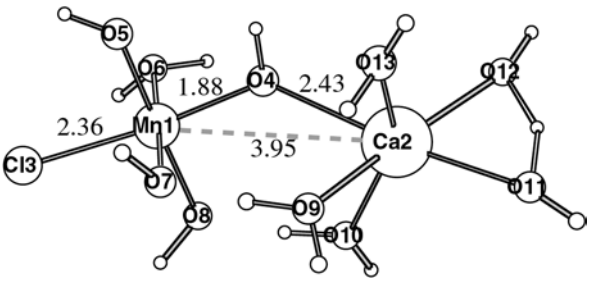

Fig. 13. Reactant used to model exchange of bridging hydroxo ligand (reaction 8). The *numbers* represent distances in angstroms

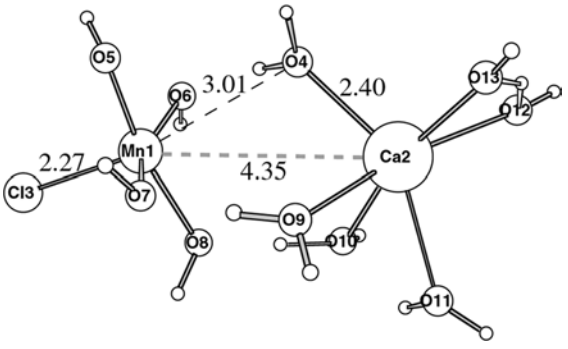

Fig. 14. TS (TS 8b) for exchange of bridging hydroxo ligand. After passing the TS, the water ends up in the coordination sphere of Ca, a position from where it can easily exchange. The *numbers* represent distances in angstroms

3.3 Exchange of the terminal oxyl radical in the Mn-dimer $[(terpy)(H_2O)Mn^{IV}(\mu\text{-}O)_2Mn^{IV}(O\bullet)(terpy)]^{3+}$ (reaction 9)

In the last part of the present study, a completely different type of exchange mechanism was modeled.

Table 2. Energies (kcal mol^{-1}) for structures along the reaction path for exchange of a hydroxo ligand. The attribution of structures (i.e. the existence of TS 8a and INT 8a) are made on the LANL2DZ energy surface. The values of ΔE do not include corrections from solvent, zero-point and thermal effects

Metal center	Reaction	TS a		INT a		TS b	
		$\Delta E^{\ddagger}$	$\Delta G^{\ddagger}$	ΔE	ΔG	$\Delta E^{\ddagger}$	$\Delta G^{\ddagger}$
$[Mn^{IV}(H_2O)_2(OH)_3(Cl)]H_2O$	3	6.3	5.2	2.1	3.0	8.6	13.6
$[(H_2O)(OH)_3(Cl)Mn^{IV}(OH)Ca^{II}(H_2O)_4(OH)]$	8	9.5	8.2	8.1	7.8	7.1	10.4

Tautomerization mechanisms for water exchange have been suggested for oxo groups on Mn porphyrins and Mn dimers [41, 42]. To continue on the Mn dimer theme, the $[(terpy)(H_2O)Mn^{IV}(\mu\text{-}O)_2Mn^{IV}(O\bullet)(terpy)]^{3+}$ dimer was chosen as a model. In the calculations, a smaller model has been used, see Fig. 15 for details. This modification did not change the structure of the dimer significantly. This dimer has two major differences compared to all previous models in the present paper. The ligands are not water-derived and the complex carries a charge since it is solvated in water.

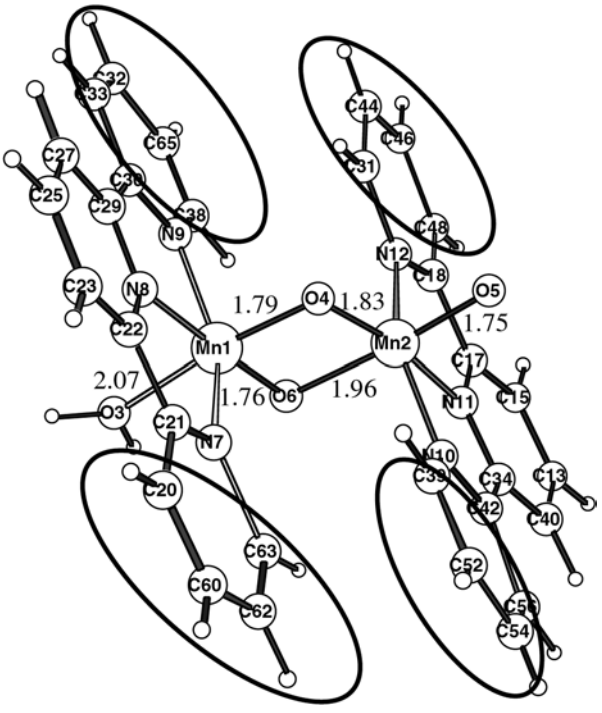

Fig. 15. Structure of the Mn dimer $[(terpy)(H_2O)Mn^{IV}(\mu\text{-}O)_2Mn^{IV}(O\bullet)(terpy)]^{3+}$. The *numbers* represent distances in angstroms. The reported distances as well as other results are from a smaller model that was obtained by replacing the *circled fragments* by terminal protons

The complex has been suggested as a functional model for photosynthetic water oxidation [42]. The active species in O–O bond formation is proposed to be a Mn^{IV}–Mn^{V} dimer with a terminal oxo group. The calculations in the present study show that it is better described as a Mn^{IV}–Mn^{IV} oxyl radical complex since the spin on the terminal oxygen is 0.82. In the following paragraphs, terminal oxyl radical will be used instead of terminal oxo group to describe this species. Mulliken spin populations of the structures involved in the tautomerization mechanism are shown in Table 3. The spin populations reported are from gas- phase calculations but values in a solvent do not differ by more than five hundredths in any case.

Isotope experiments using $H_2{}^{18}O$ suggest that the oxyl radical can exchange with water. The tautomerization reaction path proposed here is shown in Fig. 16. The reactant is the Mn^{IV}–Mn^{IV} oxyl radical complex shown in Fig. 15. The result of the tautomerization procedure is an inversion of the oxo and water ligands of reactant 9 where O3 becomes the oxyl radical and O5 becomes a water ligand that can exchange with solvent water. The product of the inversion is INT 9e in Fig. 16. Owing to the symmetry of the system, with reactant 9 and INT 9e being mirror images, the TS for the inversion is proposed to have at least C_2 symmetry.

To simplify, no external proton donors or acceptors have been included in the study of the tautomerization mechanism. Both protons supplied to O5 are provided by the other water ligand O3. The first step in the reaction is to shuffle a proton from the water ligand O3 to the oxyl radical O5. With the present model, it is not possible to calculate the barrier for this step. The result is a dimer with two terminal hydroxo groups (INT 9a) that lies 7.8 kcal mol^{-1} above the reactant. Still no Mn^{V} appears. Instead a radical has been created on the bridging oxo group O6. The Mn dimer couples antiferromagnetically with Mn1 having three α spins and Mn2 having three β spins. The radical on O6 has α spin. The

Table 3. Mulliken spin populations from gas-phase calculations (LACV3P**+ basis set) for structures along the reaction path for exchange of a terminal oxyl radical

State	Atom labels from Fig. 15					
	Mn1	Mn2	O3	O4	O5	O6
Reactant 9	2.80	−2.77	0.00	−0.06	0.82	0.15
INT 9a	2.58	−2.85	−0.29	0.33	−0.06	0.70
INT 9b	2.75	2.66	0.29	0.25	0.20	−0.97
TS 9c	2.86	2.86	0.06	−0.36	0.06	−0.36

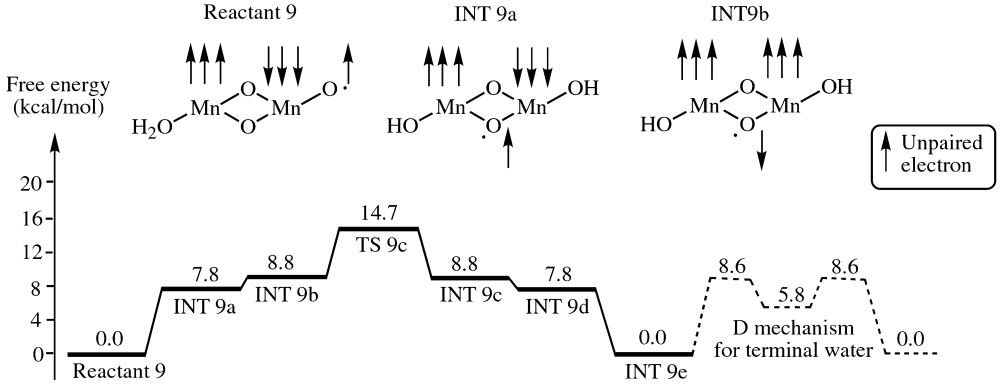

Fig. 16. Free energy diagram for the suggested tautomerization exchange mechanism of a Mn^{IV} oxyl radical on a Mn dimer. The energy for the final exchange of a terminal water is taken from previous calculations of terminal water exchange (reactant 6)

radical is associated to the O6–Mn2 bond since the distance between O6 and Mn2 is longer than the distance between O6 and Mn1.

To associate the radical to Mn1 instead of Mn2 the radical must move or spin flipping must occur. Either the spin on the radical or the spin on the Mn can flip. If the spin on O5 is flipped in reactant 9, this costs 3.5 kcal mol^{-1} more than going to ferromagnetic coupling. Therefore it is proposed that from INT 9a the Mn spins change to a ferromagnetic coupling and INT 9b is formed. No rate has been calculated for this spin transition but it is proposed to be reasonably fast owing to the large spin–orbit coupling of Mn. The sextet structure INT 9b lies 8.8 kcal mol^{-1} above reactant 9. The free-energy difference between INT 9a and INT 9b is only 1.0 kcal mol^{-1}. Looking at the electronic energy, the difference is 3.5 kcal mol^{-1} and it is corrections from solvent, zero-point and thermal effects that bring the energies of the two structures within 1 kcal mol^{-1} of each other. The spin on O6 has now increased to 0.97 and is antiparallel to both Mn1 and Mn2; however, the bond distance to Mn2 is still longer than the distance to Mn1.

To find the TS in the tautomerization mechanism, a symmetric solution is required where the bridging radical is equally associated with both Mn ions. This is accomplished by making the structure symmetric (C_{2h} symmetry) and keeping the symmetry during the geometry optimization. This gives the lowest possible energy of a symmetric solution and this should be the TS for transfer of the oxyl radical between the two Mn centers. The procedure led to TS 9c 13.7 kcal mol^{-1} above the reactant where the two bridging oxygens have equal spins. The reaction is an electron transfer where the electron moves from the bridging O6 to the bridging O4.

After passing TS 9c, the complex falls back into the unsymmetric ferromagnetic minimum INT 9c, which is a mirror image of INT 9b with the radical moved from O6 to O4. It then makes a transition back to antiferromagnetic coupling (INT 9d). Now a second proton can be transferred from O3 to O5. This is the exact reverse of the first proton-transfer step. The result is no protons at O3 and a doubly protonated O5. The former oxyl radical has become a water ligand and can now exchange with the water solvent. Without performing any calculations, it is proposed that the exchange proceeds via a D mechanism, in exact analogy with reaction 6. The energies for this step are taken from the previously modeled exchange of a terminal water ligand. The barrier is not expected to be significantly different compared to the complex with only water ligands. The terminal water is in both cases located trans to a bridging oxo group. The ligands that differ between the complexes are located cis to the water and are expected to have a lesser influence on the barrier than the common trans ligand.

As pointed out in Sect. 2, it is known that DFT does not treat open-shell low-spin states correctly. The error can be corrected as outlined in Sect. 2. For reactant 9 shown in Fig. 15, the computed J value is 0.67 kcal mol^{-1} and the correction to the low-spin state decreases the energy by 1.0 kcal mol^{-1}. Although the J value may differ between different structures, this correction is applied to both low-spin states (reactant 9 and INT 9a). The reaction barrier therefore increases by the same amount and becomes 13.7 + 1.0 = 14.7 kcal mol^{-1}. Since the spin on the radical is antiparallel to the spin on Mn, a similar correction should in principle be performed also for these spin states; however, it is assumed that this correction remains constant between reactant 9 and TS 9b since the oxygen and Mn spins stay antiparallel throughout the reaction. The potential-energy surface including the low-spin correction is shown in Fig. 16.

The $\Delta E^{\ddagger}$ and $\Delta G^{\ddagger}$ values for the exchange of a bridging oxo group and a terminal oxyl radical are shown in Table 4.

Table 4. Energy barriers (kcal mol^{-1}) for exchange of a bridging oxo group and a terminal oxyl radical (oxo group). The values of $\Delta E^{\ddagger}$ do not include corrections from solvent and thermal effects

Metal center	Reaction	$\Delta E^{\ddagger}$	$\Delta G^{\ddagger}$	Comments
$[(H_2O)_2(OH)_2Mn^{IV}(\mu\text{-}O)_2Mn^{IV}(H_2O)_2(OH)_2]$	7	19.1	19.2	Bridging oxo
$[(terpy)(H_2O)Mn^{IV}(\mu\text{-}O)_2Mn^{V}(O)(terpy)]^{3+}$	9	14.5	14.7	Terminal oxo

Unfortunately, it is not possible to compare the calculated barrier with any direct experimental measurement. What is known is that O_2 bond formation occurs with a barrier lower than 18 kcal mol^{-1} and that the exchange rate of the terminal oxyl radical is comparable to the rate of O_2 bond formation [2]. The calculated barrier is therefore consistent with experimental results although it must be admitted that the test is not very selective.

4 Discussion

The goal of the present study has been to model water-exchange reactions in proteins. However, several issues must be considered before a comparison with a real system is made.

First, metal centers in proteins have a large variety of ligands. This and previous studies have shown effects of ligand composition on exchange rates. Without specific knowledge of the ligand composition the effect remains unknown. Second, the treatment of the second coordination shell is incomplete. Hydrogen bonds between the first and the second coordination shell are likely to influence the energetics of the process. Dielectric cavity methods cannot be used as a substitute for explicit hydrogen bonds at the active site [35]. Exactly the same problem exists when exchange reactions are modeled in aqueous solution. Third, metal centers in enzymes may be subject to some strain from the surrounding protein, even though the effect is not expected to be very large. The fourth issue regards the inherent accuracy of the B3LYP method [36] as discussed in Sect. 2. Fifth, the calculations show a higher stability of the intermediates with low coordination than expected as shown by the predicted four coordination of Mn^{III}. If the calculations overestimate the stability of low-coordinated complexes, owing to an overestimation of hydrogen-bond strengths and the small size of the models, they introduce a bias towards the D mechanism. The result would be barriers that are too low. Sixth, processes other than exchange may be rate-limiting in proteins, among them diffusion of solvent water to the active site. The fast rates calculated for the monomers and terminal water ligands on dimers may never be detected experimentally. In conclusion, the present study cannot be directly compared to experimental rates at this level of modeling.

Instead the merit of the computational study is to provide results regarding effects on water-exchange rates when the metal complex is changed. All of the issues discussed in the previous paragraph are likely to have similar effects on all the modeled exchange reactions. The relative rates calculated in this work will therefore be more accurately calculated than absolute rates. All effects on the exchange rates from changing the metal complex are summarized in Table 5.

The difference between the fastest (reaction 4) and the slowest (reaction 7) exchange reaction is 12.9 kcal mol^{-1}, but many effects are in the 2-3 kcal mol^{-1} range. Are these effects significant? To answer this, the computational accuracy of the present treatment must be discussed. A previous study of the computational procedure [40] shows that adding polarization functions in the geometry optimization had only a small effect, and additional basis functions in the energy evaluation had even smaller effects. Taken together, the error is approximately 1 kcal mol^{-1} on relative energies. Another modeling problem regards the issue with multiple minima. A slightly different orientation of the hydrogens on the water and hydroxo ligands can have an effect of up to 1 kcal mol^{-1}. The stablest structure as calculated using the small basis set does not always have the lowest free energy when all corrections are added. Although many attempts have been made both for dimer and monomer reactants, there is no guarantee that the stablest structure has been found. A related problem regards the choice of reactant. As already stated, different choices of reactant were made for the monomer and the dimer. For the monomer, the global minimum was chosen and the complex was allowed to rotate its ligands as it approaches the TS. The same freedom of rotation is not always available for the dimers. In these cases, the choice of reactant was the lowest-energy structure on the potential surface that leads directly to the TS.

Taken together, the errors for any given change in the barrier when the metal complex is modified may be around 1–2 kcal mol^{-1}. This is accurate enough to draw general conclusions regarding the differences shown in Table 5.

First looking at the monomers, the Cl^- ligand raises the barrier by 1.2 (Mn^{IV}) or 3.2 kcal mol^{-1} (Mn^{III}). An interpretation is that the high electron affinity of Cl draws electrons towards this ligand. This increases the charge on the Mn center and stabilizes the other ligands. The magnitude of the effect is reasonable for Mn^{IV} but it is very large for Mn^{III}. This indicates an error in any of the two structures compared as argued previously. The barrier for exchange on Mn^{III} is 3.3 kcal mol^{-1} lower

Table 5. Effects on the reaction barriers (kcal mol^{-1}) of the different modifications modeled in the present paper. The values of $\Delta\Delta E^{\ddagger}$ do not include corrections from solvent and thermal effects

Modification	Reactions compared	$\Delta\Delta E^{\ddagger}$	$\Delta\Delta G^{\ddagger}$
Add Cl^- ligand to Mn^{IV}	2 and 1	1.2	1.2
Exchange OH^- instead of H_2O	3 and 2	−0.2	2.8
Exchange on Mn^{III} instead of Mn^{IV}	4 and 1	−1.7	−3.3
Add Cl^- ligand to Mn^{III}	5 and 4	1.3	3.2
Exchange water on dimer instead of monomer	6 and 1	0.8	−1.0
Exchange bridging oxo instead of terminal water	7 and 1	10.7	10.6
Exchange OH^- when Ca chelates	8 and 3	−1.5	−3.2
Exchange terminal oxyl radical instead of terminal water	9 and 6	6.1	5.4

than on Mn^{IV}. The effect is expected both owing to the lower oxidation state and owing to the presence of a JT axis in Mn^{III}. The absolute value of the Mn^{III} exchange barrier (6.3 kcal mol^{-1}) is rather close to the guess from the Introduction (6.9 kcal mol^{-1}). Exchange of a hydroxo ligand has a reaction barrier that is 2.8 kcal mol^{-1} higher than the barrier for exchange of water on the same center. Looking only at the electronic energy, the energies are almost the same for exchange of water and hydroxide. This is difficult to explain but the result is more reasonable when the solvent effects are added. The difference in rates between water and hydroxide depends on the available proton donors in the surroundings. By adding Ca, the barrier for exchange of OH^- decreases significantly ($\Delta\Delta G^{\ddagger} = -3.2$ kcal mol^{-1}). The effect of Ca is interesting. It seems to stabilize the TS by providing a flexible coordination.

Continuing to dimers, the terminal ligand of the Mn^{IV}–Mn^{IV} dimer exchanges with a barrier 1.0 kcal mol^{-1} lower compared to a water ligand on the monomer. This may be due to the trans effect of the bridging oxo. Comparing exchange rates between bridging and terminal positions is difficult. Looking at the model complex, the oxo bridge exchanges significantly more slowely than the terminal water (barrier of 19.2 versus 8.6 kcal mol^{-1}). When looking at complexes with other ligands, the result for exchange of the bridging oxo is very uncertain. It should be remembered that if the energy to protonate the bridge to a hydroxo group is endothermic, it should be included in the barrier. In this study, it has been shown to vary by approximately 7 kcal mol^{-1} between the two complexes studied, although only 4 kcal mol^{-1} would have an effect on the barrier. The availability of proton donors in the protein will also have an effect on the rate. In contrast, the barrier for exchange of a terminal water should be stable when it comes to a change in ligand composition. The exchanging terminal water in a μ-oxo dimer will always have an oxo group in the trans position, despite the ligand composition. Ligands in cis positions have a smaller effect on the exchange rate. Exchange of a terminal oxyl radical is also slow compared to exchange of a terminal water ($\Delta\Delta G^{\ddagger} = 6.1$ kcal mol^{-1}).

Since most effects obtained when changing the metal complex seem reasonable, it is interesting to compare the results with the water-exchange experiments performed on the Mn_4 complex in PSII [2]. Most significant is a discussion of the changes when going between various S states. To make any interpretations from the models, it must be assumed that other processes, i.e. large changes in the protein environment, are not the origin of the changes in exchange rate.

The two water molecules that are oxidized during the reaction exchange independently and with different rates. One of the water molecules exchanges more slowly than the other one, in all S states. Beginning with the S_0 state, the slowest of the two exchanges with a barrier of 15.4 kcal mol^{-1}. Despite using caution when comparing experimental and calculated rates it seems unlikely that this is a terminal position. The experimental barrier is 7 kcal mol^{-1} higher than the calculated barrier for terminal water exchange and it is not likely that a terminal ligand is highly oxidated in the S_0 state. It has been argued already that the results for terminal exchange are less prone to errors due to unknown ligand compositions than other barriers and an error of 7 kcal mol^{-1} or more seems unlikely. The remaining alternatives are exchange of a hydroxo group or a bridging oxo group. In the S_1 state, the barrier increases to 18.7 kcal mol^{-1}. The increase in barrier when going from S_0 to S_1 is consistent with a change in the oxidation state of Mn or the loss of a proton. The match between the barrier in the S_1 state (18.7 kcal mol^{-1}) and the calculated 19.2 kcal mol^{-1} for a bridging group in a Mn^{IV}–Mn^{IV} dimer must be regarded as somewhat circumstantial. In the next transition (S_1 to S_2) the exchange rate increases and the barrier drops by 2.6 kcal mol^{-1}. This result is maybe the most interesting of all the results obtained, but it is difficult to explain. A tentative explanation is that in this step, Ca changes its coordination and binds to the ligand. The exchange rate stays the same in the S_2 and S_3 states, which indicates that oxidation occurs at a position far from the exchanging water.

The rapidly exchanging water molecule is a different case. In all different S states, the barrier is lower than 14.5 kcal mol^{-1}. A suggestion is that this water molecule is a terminal ligand or does not bind significantly until later S states. Processes other than exchange from Mn will then be rate-limiting, for example, diffusion of water to the active site. The changes in the barrier are too small to be well described by the present models. The idea that the two water molecules bind to significantly different positions is supported by the entropy effects that can be obtained from exchange data recorded in the S_3 state [43]. The slowly exchanging water ligand has an entropy effect that decreases the barrier by 2 kcal mol^{-1}, while the rapidly exchanging water has an entropy effect that raises the barrier by almost 5 kcal mol^{-1}. In the present calculations, the entropy effect lowers the barrier for exchange of a μ-oxo bridge by 2.4 kcal mol^{-1}. This is rather close to the value obtained by experiments. On the other hand, no calculation in this study has reproduced the large entropy effect observed for the rapidly exchanging water.

5 Summary

Reaction barriers for water exchange on metal centers have been calculated. The most interesting results regard exchange of oxo groups and water ligands on Mn dimers. A bridging oxo group exchanges with a ring-opening mechanism and the reaction barrier is 19.2 kcal mol^{-1}. This value is uncertain but compares favorably to the exchange of one of the oxygens in the S_1 state of the OEC in PSII. Terminal water ligands and water ligands on monomers are predicted to exchange very rapidly.

References

1. Helm L, Merbach AE (1999) Coord Chem Rev 187: 151–181
2. Hillier W, Wydrzynski T (2000) Biochemistry 39: 4399–4405
3. Zouni A, Witt H-T, Kern J, Fromme P, Krauss N, Saenger W, Orth P (2001) Nature 409: 739–743

4. Barynin VV, Hempstead PD, Vagin AA, Antonyuk SV, Melik-Adamyan WR, Lamzin VS, Harrison PM, Artymiuk PJ (1997) J Inorg Biochem 67: 196
5. Nordlund P, Sjöberg B-M, Eklund H (1990) Nature 345: 593–598
6. Yachandra VK, Sauer K, Klein MP (1996) Chem Rev 96: 2927–2950
7. Siegbahn PEM (2000) Inorg Chem 39: 2923–2935
8. Langford CH, Gray HB (1966) Ligand substitution processes. Benjamin, New York, pp 7–11
9. Merbach AE (1982) Pure Appl Chem 54: 1479–1493
10. Rotzinger FP (1997) J Am Chem Soc 119: 5230–5238
11. Ducommun Y, Newman KE, Merbach AE (1980) Inorg Chem 19: 3696–3703
12. Tsutsui Y, Wasada H, Funahashi S (1999) J Mol Struct (THEOCHEM) 461–462: 379–390
13. Deeth RJ, Elding LI (1996) Inorg Chem 35: 5019–5026
14. Hartmann M, Clark T, van Eldik R (1997) J Am Chem Soc 119: 7843–7850
15. Hartmann M, Clark T, van Eldik R (1999) J Phys Chem A 103: 9899–9905
16. Vallet V, Wahlgren U, Schimmelpfennig B, Szabó Z, Grenthe I (2001) J Am Chem Soc 123: 11999–12008
17. Bleuzen A, Foglia F, Furet E, Helm L, Merbach AE, Weber J (1996) J Am Chem Soc 118: 12777–12787
18. Rotzinger FP (2000) Helv Chimi Acta 83: 3006–3020
19. Klamt A, Schuurmann G (1993) J Chem Soc Perkin Trans 25: 799–805
20. Barone V, Cossi M (1998) J Phys Chem A 102: 1995–2001
21. Xu F-C, Krouse HR, Swaddle TW (1985) Inorg Chem 24: 267–270
22. Crimp SJ, Spiccia L, Krouse HR, Swaddle TW (1994) Inorg Chem 33: 465–470
23. Plumb W, Harris GM (1964) Inorg Chem 3: 542–545
24. Drjlaca A, Zahl A, van Eldik R (1998) Inorg Chem 37: 3948–3953
25. Hurst JK, Zhou J, Lei Y (1992) Inorg Chem 31: 1010–1017
26. Yamada H, Hurst JK (2000) J Am Chem Soc 122: 5303–5311
27. Sjöberg B-M, Loehr TM, Sanders-Loehr J (1982) Biochemistry 21: 96–102
28. Becke AD (1993) J Chem Phys 98: 1372–1377
29. Becke AD (1993) J Chem Phys 98: 5648–5652
30. Frisch MJ, Trucks GW, Schlegel HB, Scuseria GE, Robb MA, Cheeseman JR, Zakrzewski VG, Montgomery JA, Stratman RE, Burant JC, Dapprich S, Millam JM, Daniels AD, Kudin KN, Strain MC, Farkas O, Tomasi J, Barone V, Cossi M, Cammi R, Mennucci B, Pomelli C, Adamo C, Clifford S, Ochterski J, Petersson GA, Ayala PY, Cui Q, Morokuma K, Malick DK, Rabuck AD, Raghavachari K, Foresman JB, Cioslowski J, Ortiz JV, Baboul AG, Stefanov BB, Liu C, Liashenko A, Piskorz P, Komaromi I, Gomperts R, Martin RL, Fox DJ, Keith T, Al-Laham MA, Peng CY, Nanayakkara A, Gonzalez C, Challacombe M, Gill PMW, Johnson BG, Chen W, Wong MW, Andres JL, Gonzales C, Head-Gordon M, Replogle ES, Pople JA (1998) Gaussian 98. Gaussian, Pittsburgh, PA
31. Schrödinger Inc (1991–2000) Jaguar 4.1. Schrödinger, Portland, OR
32. Dunning TH Jr, Hay PJ (1976) In: Schaefer HF (ed) Methods of electronic structure theory. Modern theoretical chemistry, vol 3. Plenum, New York pp 1–28
33. Hay PJ, Wadt WR (1985) J Chem Phys 82: 299–310
34. Siegbahn PEM (1996) In: Prigogine I, Rice SA (eds) New methods in computational quantum mechanics. Advances in chemical physics, vol. XCIII, Wiley Interscience, New York pp 333–387
35. Blomberg MRA, Siegbahn PEM, Babcock GT (1998) J Am Chem Soc 120: 8812–8824
36. Curtiss LA, Raghavachari K, Redfern RC, Pople JA (2000) J Chem Phys 112: 7374–7383
37. Noodleman L, Case DA (1992) Adv Inorg Chem 38: 423–470
38. Blomberg MRA, Siegbahn PEM (1997) Theor Chem Acc 97: 72–80
39. van Eldik R (1999) Coord Chem Rev 182: 373–410
40. Siegbahn PEM (2001) J Comput Chem 22: 1634–1645
41. Bernadou J, Meunier B (1998) Chem Commun 20: 2167–2173
42. Limburg J, Vrettos JS, Chen H, de Paula JC, Crabtree RH, Brudvig GW (2001) J Am Chem Soc 123: 423–430
43. Hillier W, Messinger J, Wydrzynski T (1998) Biochemistry 37: 16908–16914